POLITECNICO
MILANO 1863

DIPARTIMENTO DI MECCANICA

mecc

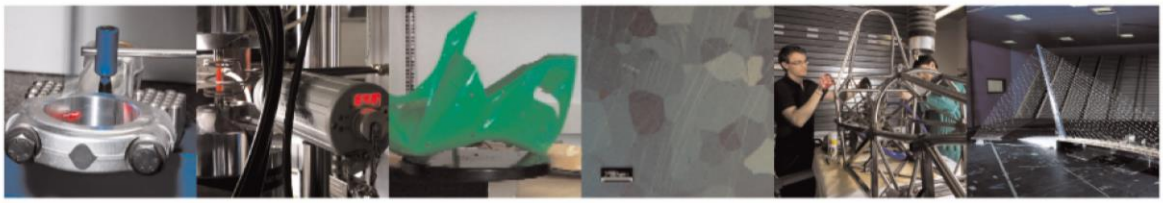

A novel prognostics solution for machine tool sub-units: The hydraulic case

Bernini L, Waltz D, Albertelli P, Monno M.

This is a post-peer-review, pre-copyedit version of an article published in Bernini L, Waltz D, Albertelli P, Monno M. A novel prognostics solution for machine tool sub-units: The hydraulic case. Proceedings of the Institution of Mechanical Engineers, Part B: Journal of Engineering Manufacture. December 2021. doi:10.1177/09544054211064682. The final authenticated version is available online at: http://dx.doi.org/10.1177/09544054211064682

DIPARTIMENTO DI MECCANICA ■ POLITECNICO DI MILANO
via G. La Masa, 1 ■ 20156 Milano ■ EMAIL (PEC): pecmecc@cert.polimi.it
http://www.mecc.polimi.it
Rev. 0

A novel prognostics solution for machine tool sub-units: the hydraulic case.

Journal Title
XX(X):1–19

DOI: 10.1177/ToBeAssigned
www.sagepub.com/
SAGE

Luca Bernini[1,2], David Waltz[1,2], Paolo Albertelli[1,2] and Michele Monno[1,2]

Abstract

A novel prognostic approach was developed and applied to a machine tool hydraulic unit. Three components were considered: pump, sensor and valve. The proposed methodology exploited a digital twin of the system to perform simulations of the healthy and faulty machine. The digital twin was properly validated through experiments. This approach dealt with the need to carry out time-consuming and expensive experimental campaigns, i.e. run-to-failures - not affordable in many industrial applications. The diagnosis module was trained on digital twin simulations and fulfilled the fault detection, isolation and quantification phases. The challenge related to the variability of the operating conditions of the machine was addressed through a robustness analysis of the methodology. The solution successfully dealt with both stationary and non-stationary working conditions. A dedicated classification model was designed for each faulty component, maximising the associated classification rate. The testing procedure consisted of the application of a 10-fold cross-validation to compute the mean classification rates for stationary and non-stationary working conditions. Diagnosis performance results were excellent for the pump, whereas they were lower for the sensor and valve, reaching 79.75% and 74.93% accuracy respectively for the most challenging working cycle. The prognosis directly exploited the output of diagnostics, allowing for experimental effort reduction. Prognosis predictions were built starting from the updated health status provided by the diagnosis output. In order to test the prognosis module, mean and standard deviation of the prediction errors (less than 1.176%) were computed through a Monte Carlo approach. The conceived methodology allowed one of the critical goals of prognostics to be handled: the Remaining Useful Life probability density function estimation.

Keywords

Prognostics, Diagnostics, Machine Tools, Digital Twin, Hydraulic Units

1 Introduction

In manufacturing systems, productivity targets are demanding to ensure maximum reliability and availability of machine tools[1], while breakdowns and failures need to be fully avoided[2,3]. Due to these requirements and increased system complexity, preventive maintenance represents a conspicuous fraction of the total costs in an industrial scenario[4]. Consequently, the attractiveness of Prognostics and Health Management (PHM) solutions rises.

International standards describe the PHM framework[5–9] that consists of four modules: preliminary analysis, profile monitoring, diagnosis and prognosis[10]. The first regards the collection and investigation of all possible faults of the analysed system. The second performs the fault detection, i.e. the observation of a statistical discrepancy between the ongoing and a pre-recorded healthy working condition. The third deals with fault isolation and quantification, i.e. the localisation of the faulty component and its wear level assessment, respectively. The last step deals with the prediction of the Remaining Useful Life (RUL) of the component, i.e. the remaining time for which the component can perform the assigned task. RUL estimation should also contain information about its uncertainty through the estimation of its probability density function (pdf)[10].

Two steps are needed to create a proper dataset for PHM strategies: feature extraction and feature selection. The first

[1]Department of Mechanical Engineering, Politecnico di Milano, via La Masa 1, 20156 Milan, Italy.
[2]MUSP Macchine Utensili Sistemi di Produzione, strada della Torre della Razza, 29122 Piacenza, Italy

Corresponding author:
Luca Bernini, Department of Mechanical Engineering, Politecnico di Milano, via La Masa 1, 20156 Milan, Italy.
Email: luca1.bernini@polimi.it

consists of the computation of statistical quantities from sensor data. It enables dimensionality reduction of collected data, trying to condense the information as much as possible. Features can be computed in many domains: time, frequency and time-frequency domain[4,11,12]. Feature selection allows for a further reduction of the features pool. Spearman's and Pearson's correlation coefficients can be used to rank features and keep the most correlated ones[11,12]. ANOVA could be applied when data are collected in classes[13].

Once the dataset is created, profile monitoring techniques can be adopted. Statistical Process Control (SPC)[14] is the typical tool, as proposed by Liu *et al.*[15] and Colosimo *et al.*[16].

Diagnosis is a classification problem. Several types of algorithms could be used to localise and identify the nature of the fault: Linear Discriminant Analysis (LDA), Support Vector Machines (SVM)[17], Mahalanobis-Taguchi Systems[18], filtering techniques, e.g. Unscented Kalman Filter (UKF)[19] and Artificial Neural Networks (ANN) are just a subset of possible solutions[11,20,21]. An innovation in this field could be progressive learning, introducing the capability of increasing the number of clusters during online learning[22]. Additionally, utility theory can be applied to introduce probabilities of critical conditions. It was successfully implemented to support decision making in maintenance actions on bearing faults in a sewage treatment plant[17].

Dealing with prognostics, four main algorithm categories can be distinguished depending on the data availability and the approach to the problem[10,23]:

- Knowledge-based models: expert knowledge is translated in simple rules that the system can interpret. Such methods can be used only if robust knowledge of the degradation phenomenon and the machine is available. Expert systems, in which rules assume the form of *IF-THEN*, and fuzzy logic, giving a linguistic description of the system, are part of this category[10,23];
- White-box models (model-based): they rely on a physical model of the degradation phenomenon[23]. Although the model structure is known *a priori*, experimental data are necessary to identify the model parameters[10]. Exponential lifetime prediction model for ball screw mechanisms under different feed modes[24], differential models for tool wear evolution in milling[25] and wear model for flank wear in turning[26] are just examples of this;
- Grey-box models (statistical-based methods): they rely on a dynamic stochastic description of the degradation phenomenon. The model is selected by the user and its coefficients are estimated through experimental data[10]. Their advantage is related to a statistical description of the RUL and, indeed, a strong support for decision making on maintenance actions. Filtering-based approaches such as Kalman filters[27] and its variations[28], or particle filters[29,30] are all examples of grey-box approaches, as well as Hidden Markov Models (HMM) and Hidden semi-Markov Models[10]. Linear regression models can even be applied for RUL prediction[31].
- Black-box models (data-driven): they "learn" and describe the problem directly from the collected data. Data quantity and quality of both faulty and fault-free data are of fundamental importance for successful implementation[5]. ANN, Self-Organising-Maps (SOM)[15,32,33] and deep learning algorithms, SVM and Relevance Vector Machines (RVM)[34] are just a few examples of artificial intelligence techniques.

Hybrid approaches have recently emerged, fusing multiple areas and exploiting their synergies. For instance, Sbarufatti *et al.* developed a prognostic solution for Li-ion batteries using particle filters to update Radial Basis Function Neural Networks. This solution could predict the RUL pdf, providing adaptiveness to new data[35].

Actually, different challenges prevent PHM techniques to find a robust implementation in manufacturing:

- the system under analysis needs to be sensorised to provide meaningful signals regarding the fault conditions. No rules have been designed to choose the right ones;
- experimentation is needed: all the techniques available nowadays require training data (data from all the fault combinations or run-to-failures). Typically, only fault-free data are largely available and experimentation can be extremely expensive and time-consuming;
- developed solutions are often working-cycle dependent. This is a critical problem in many applications, e.g. with machining centres;
- how to estimate and deal with the uncertainty of the RUL prediction, i.e. the determination of its pdf.

Furthermore, scientific research is still lacking in the manufacturing field. The hydraulic unit is one of the most critical parts and the cause of unexpected breakdowns and downtimes[1,3]. From a reliability analysis of ten CNC lathes from 2009 to 2014, the hydraulic subsystem showed the highest failure rate (22.9% of the total failures)[1]. A similar project on twelve machining centres between 2005

and 2010 confirmed the result[36]. Two other contributions highlighted the necessities of performing PHM on machine tool auxiliaries, being sources of unexpected downtimes and of comparable loss of production costs with respect to machine tool main components[37,38]. Despite the above, research on PHM of CNC machines is rare in such subsystems, especially on hydraulic units. A case study on monitoring the filter's health state in an oil mist separator was recently presented in 2019[37]. Authors trained machine learning on healthy data to model the environmental effects on the measured fan power. The reconstruction error was used as the health index (HI) of the filter. Instead, PHM in the machine tools field mainly focuses on tool monitoring and prognostics. Specific force coefficients were addressed as cutting-condition independent and tool-wear sensitive features by Nouri *et al.*[39]. Cheng *et al.* proposed a machine learning methodology based on cutting forces, vibration signals and machined surfaces' image features, typically used separately, to monitor the wear of different turning tools over various materials and cutting conditions[40]. McLeay *et al.* applied a Mahalanobis distance-based unsupervised algorithm to detect anomalies in the cutting process to assess the tool life in milling applications under fixed working conditions. The advantage of being an unsupervised method relies on the fact that only the normality condition is experimented for the training phase[41]. DaSilva *et al.* investigated tool wear evolution in the drilling of high-strength compacted graphite cast irons and individuated the spindle current signal as the best cost-benefit monitoring variable for tool wear[42]. HMM were also applied in different fashions for tool wear applications[43,44]. Other subsystems are investigated by research literature to a lesser extent, such as those of the spindle and feed-drive. Chen *et al.* developed an overall machine tool monitoring method based on the frequency analysis of energy, intended as the collection of power, thermal, current and vibration measurements. Analytical modelling of screw, guide rail and bearing frequencies allowed the health status of the components to be estimated[45]. Moore *et al.* presented a test scenario in which machine learning and deep learning classifiers were applied for machining defects and machine tool failure-mode classification. Besides this, unsupervised algorithms for clustering were tested for novel failure-mode recognition[46]. Xia *et al.* developed a diagnosis solution for multiple units of flexible production line machining centres, including feed axes, spindles and converters. A neural network scheme was adapted to each machining centre to avoid the combination explosion of learning rules and miss-classification[47]. Multiple polynomial regression[48], the Mahalanobis-Taguchi System[49] and SOM[30] were applied to predict the RUL of rolling element bearing failures in the spindle system. Feed-drive system health and its influence on tool wear was investigated through a long-term operational modal analysis of vibration signals[50].

The focus of this paper is mainly concentrated on the challenges mentioned above. A novel approach to deal with PHM was presented, trying to avoid run-to-failures through the use of a Dymola® model of the hydraulic unit of a machine tool. In section 2, the system and the model were described, together with its validation. The proposed solution was explained in section 3, supported by a graphical representation of the whole approach. Starting from the simulation of different working regimes (3.1), the creation of the datasets was described in subsection 3.2. The novel structure of the diagnostics phase, exploiting different algorithms for any component, was presented in subsection 3.5. In subsection 3.6, the innovative developed prognosis algorithm was presented, being set free from run-to-failures. Lastly, in section 4, a critical analysis of the entire process was carried out, while future developments and conclusions were reported in section 5.

Nomenclature

aux	Pump controller auxiliary variable
b	Sensor bias for sensor offset fault
dh	Fluid specific enthalpy difference between component ports
dp	Fluid pressure drop in a component
e	Prediction error
e^D	Prediction error sample distribution
h	Fluid specific enthalpy in a component port
$\dot{m}$	Fluid mass flow rate through a component
n	Numerosity of a group/fault combination
p	Fluid pressure in a component port
pos	Spool position in a valve
r	Number of groups/fault combinations used for training
$rate$	Constant degradation rate in a piece of Monte Carlo simulations
$t_{EoL,true}$	Real time of End of Life of a component

$\hat{t}^{-}_{EoL}, \hat{t}^{+}_{EoL}$ Lower and upper estimates of time of End of Life

$\hat{t}^{PE}_{EoL}$ Point estimate of End of Life

t_i Time at which diagnosis output of a component changes

th_l, th_u Lower and upper pump controller pressure limits

$x_{ij,k}$ Feature k value of the i-th simulation in group j

$\overline{x}_{j,k}$ Mean of feature k in group j

$\overline{x}_k$ Mean of feature k

A_v Valve coefficient

$Cov(\cdot,\cdot)$ Sample covariance operator

F One-way ANOVA F-statistic of a feature

HI Health index of a component

HI^-, HI^+ Lower and upper estimates of health index

$HI^-(t_i), HI^+(t_i)$ Lower and upper estimates of health index at time t_i

M Number of Monte Carlo simulations

N Total number of dataset rows/simulations

P Pump power

V_{disp} Pump displacement

$\dot{V}$ Volumetric flow rate

δHI Gap between classification output levels

η_g Pump global efficiency

η_v Pump volumetric efficiency

μ_t, μ_r Means of piece duration and degradation rate in Monte Carlo simulations

ρ Fluid density in a component port

$\rho_{k,m}$ Correlation coefficient between two features

σ Sample standard deviation of a feature

σ_t, σ_r Standard deviations of piece duration and degradation rate in Monte Carlo simulations

τ Pump shaft torque

ϕ Pump shaft angular position

ω Pump shaft angular speed

Δt_d Diagnosis cycle time

Δt Duration of a piece at constant degradation rate in Monte Carlo simulations

2 Materials

2.1 System and model description

The system is the hydraulic unit of Mandelli's Spark machining centres. It is constituted by a high pressure (HP) sub-unit (that drives the tool clamping system and the braking system); a medium pressure sub-unit (that cools down and lubricates the biggest organs in the machine); a low pressure sub-unit (that cools down the oil by pumping it to the chiller).

One of the novelties at the basis of this research was to reproduce the faulty behaviour of the system through simulations. All the described sub-units were modelled together with different fault states of the system. A schematic representation of the digital twin developed in Dymola® was shown in figure 1.

In order to focus only on relevant faults, the history of 15 years of maintenance reports was analysed. They contained data from several similar machines and different faults. The evolution of the fault occurrences over the 15 years was shown in figure 2. Although filter faults were the ones that occurred the most, they were typically subject to ordinary maintenance. Then, pump, sensor and valve faults were the most frequent and relevant ones. A HP pump leakage (fig. 1a), a pressure-switch offset (fig. 1b) and an increased opening time for the servo-valve of the tool clamping actuators (fig. 1c) were introduced in the model of the system [11,51]. The pump was a positive displacement VIVOIL XV1/P-4.9D. The sensor, the subject of the analysis, was a pressure-switch used to keep the HP system between 85 and 95 bar. The HP pump was controlled in a closed-loop by this sensor (IFM PN7071 025-MPa).

The HP pump was modelled through the following equations:

$$\omega = \frac{d\phi}{dt} \tag{1}$$

$$\tau = \frac{V_{disp} \cdot dp \cdot \eta_v}{2\pi \cdot \eta_g} \tag{2}$$

where ω and ϕ are the angular speed and position of the pump shaft, respectively; τ is the torque applied to the shaft; V_{disp} is the displacement of the pump; dp is the pressure difference between the pump ports; η_v and η_g are the volumetric and global efficiencies, respectively. The mass balance equation is:

$$\dot{m}_{in} = -\dot{m}_{out} = \dot{m} \tag{3}$$

where $\dot{m}_{in}$ and $\dot{m}_{out}$ represent the mass flows at the inlet and outlet pump ports respectively; $\dot{m}$ is the module and the minus sign represents a flow exiting the port. Specific

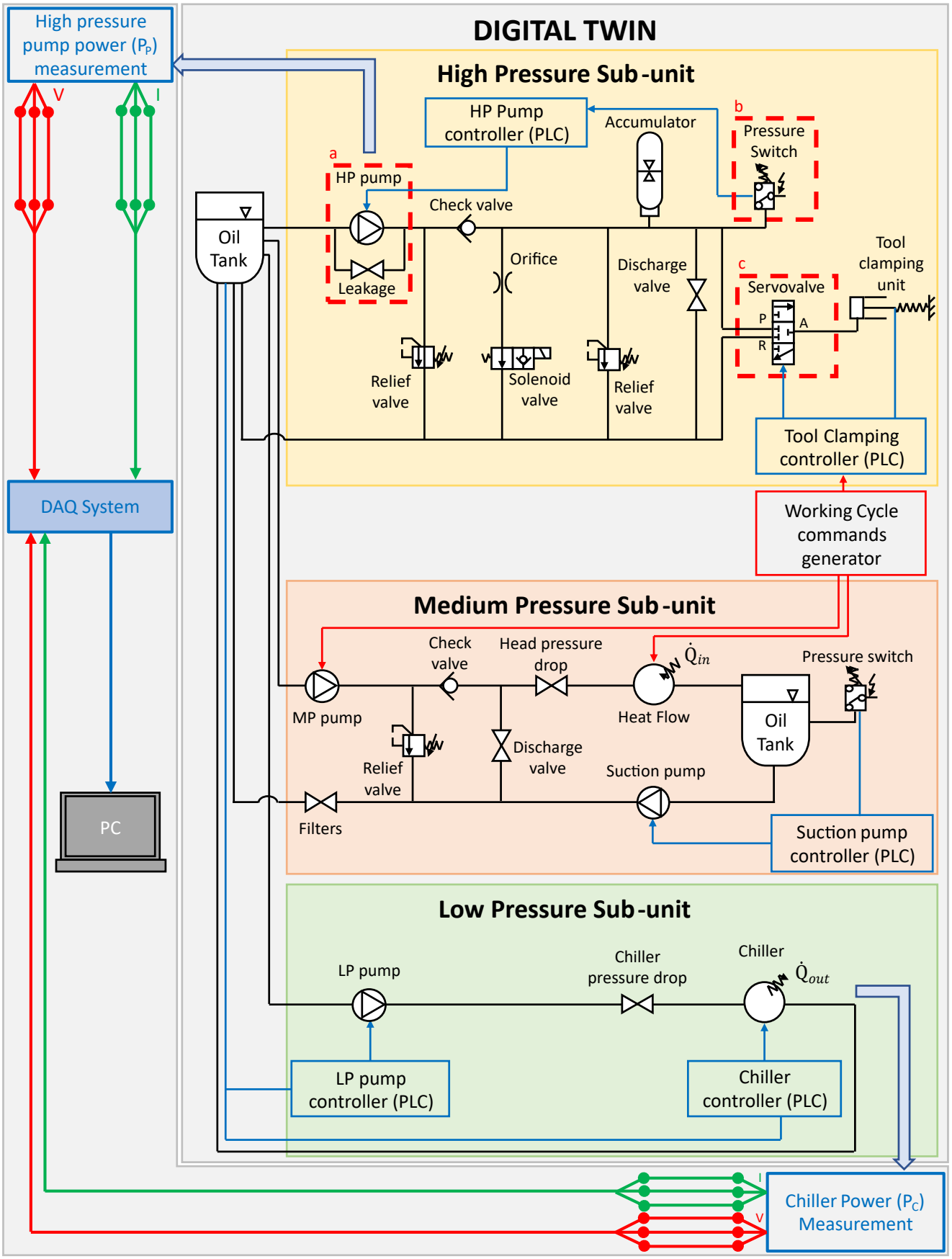

Figure 1. Digital twin layout. Top-left and bottom right arrows represent the link from the digital twin to the measurement system. In the three dashed boxes, the components under analysis: a) HP pump; b) Pressure-switch; c) Servovalve

enthalpies at the two ports are related to pressures by:

$$p_{out} = p_{in} + dp \tag{5}$$

$$h_{out} = h_{in} + dh \tag{4}$$

Table 1. Fault states and associated HI for each component.

Pump Leakage ($\frac{\dot{m}_l}{\dot{m}_{nom}}100$ [%])	HI_P [%]	Sensor offset [bar]	HI_S [%]	Valve natural frequency [Hz]	HI_V [%]
0.0	100	0.0	100	29.8	100
0.6	80	0.5	80	25.0	50
1.2	60	1.0	60	21.2	0
1.8	40	1.5	40		
2.4	20	2.0	20		
3.0	0	2.5	0		

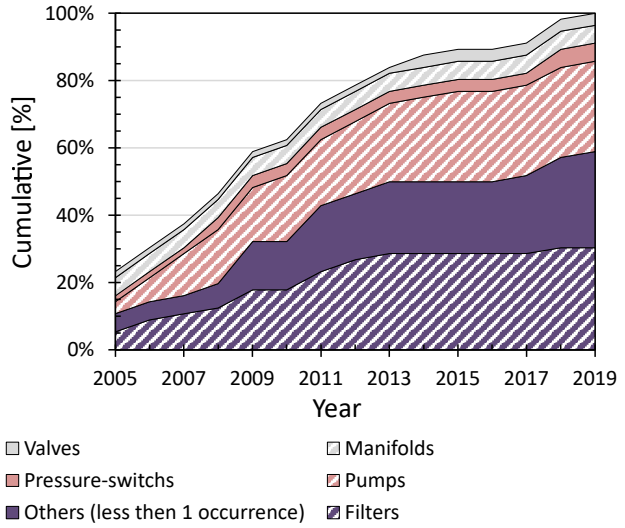

Figure 2. Evolution of fault occurrences over the 15 years maintenance reports

$$\rho_{in} = \rho \tag{6}$$

$$dh = \frac{dp}{\rho \cdot \eta_g} \tag{7}$$

where ρ is the working fluid density, defined as the inlet port oil density ρ_{in}. The mass flow and the pump power are:

$$\dot{m} = \rho \cdot \dot{V} = \frac{\rho \cdot \eta_v \cdot V_{disp} \cdot \omega}{2\pi} \tag{8}$$

$$P = \dot{m} \cdot dh \tag{9}$$

The pump leakage was introduced in the model as a valve described by the following equations:

$$\dot{m}_{leakage} = pos_{leakage} \cdot A_v \cdot \sqrt{dp \cdot \rho} \tag{10}$$

$$A_v = \frac{\dot{m}_{nom}}{\sqrt{dp_{nom} \cdot \rho_{nom}}} \tag{11}$$

where $\dot{m}_{leakage}$ is the leakage flow; A_v is the valve coefficient; dp_{nom}, ρ_{nom} and $\dot{m}_{nom}$ are nominal values for the fully opened valve; $pos_{leakage}$ represents the opening degree of the valve and regulates the leakage flow.

Since the pressure switch is a sensor, its output is just the pressure of the oil at the inlet port. It commands the HP pump through an on/off switch. It turns on the pump when the pressure decreases below the lower threshold th_l, whereas it turns off the pump when the pressure increases over the upper threshold th_u. Being aux an auxiliary variable:

$$aux = \begin{cases} th_l, & \text{when } p <= th_l \\ th_u, & \text{when } p >= th_l \end{cases} \tag{12}$$

where p is the pressure measured by the pressure switch. If p is outside the two control thresholds th_l and th_u, the command y is:

$$y = \begin{cases} 1, & \text{if } p <= th_l \\ 0, & \text{if } p >= th_u \end{cases} \tag{13}$$

If p is in between the two control thresholds, then:

$$y = \begin{cases} 0, & \text{if } aux > \frac{th_l + th_u}{2} \\ 1, & \text{otherwise.} \end{cases} \tag{14}$$

The pressure switch offset was introduced by adding a bias to the real pressure of the system, so that:

$$p = p_{real} + b \tag{15}$$

where p is the actual reading of the sensor, p_{real} is the real pressure at the sensor inlet port and b is the bias term.

The servovalve was modelled as two separated valves with complementary opening positions. The first one linked the HP port P to the actuator port A, the second one linked the actuator port A to the return line R (fig. 1c). The equations governing the servovalve behaviour are:

$$\dot{m}_{PA} = pos_{PA} \cdot A_v \cdot \sqrt{dp \cdot \rho} \tag{16}$$

$$\dot{m}_{AR} = pos_{AR} \cdot A_v \cdot \sqrt{dp \cdot \rho} \tag{17}$$

$$A_v = \frac{\dot{m}_{nom}}{\sqrt{dp_{nom} \cdot \rho_{nom}}} \tag{18}$$

where $\dot{m}_{PA}$ and $\dot{m}_{AR}$ are the oil flows through the valves; A_v is the valve coefficient; dp_{nom}, ρ_{nom} and $\dot{m}_{nom}$ are

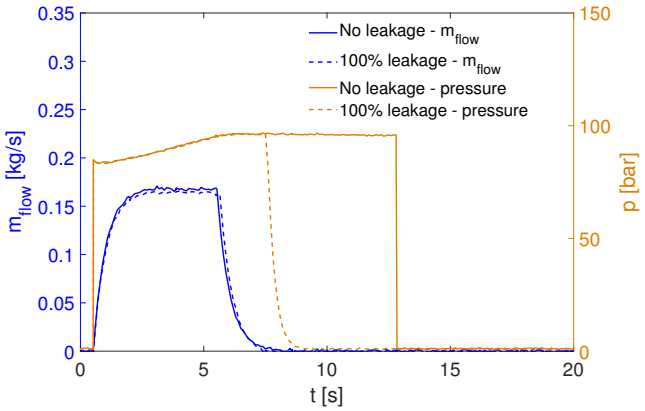

Figure 3. Comparison between pressures and mass flows of the HP pump with and without leakage fault

nominal operating points for fully opened valves. pos_{PA} and pos_{AR} are second order dynamic responses[52] to the positioning error of the actuator normalised on the actuator stroke. They are constrained to be in the range of 0 and 1. The servovalve fault was introduced by changing the natural frequency of the second order transfer functions. The simulated fault states, with the associated HI were reported in table 1. An example of the difference in the physical quantities of the system caused by the faults was shown in figure 3. The pressure at the outlet of the HP pump and the mass flow of the pump were compared in a full-health behaviour and in the 100% pump leakage case. The leakage implied a longer time to reach the required pressure and the pressure at the outlet port was quickly discharged.

2.2 Digital twin experimental validation

The validation of the digital twin was conducted by means of power acquisitions performed on a Mandelli's Spark 1600 machining centre:

- power absorbed by the HP pump electric motor;
- power absorbed by the chiller;

The experimental setup (fig. 4) was composed of a three-phase acquisition system for phase voltages and currents for each of the above units. Six LEM LF 205-S/SP3 and three NI9205 acquisition cards from National Instruments™ were adopted.

A brief comparison between the experimental and the simulated physical quantities during a healthy cycle was shown in figure 5a. Both the duty cycle and power consumption of the HP pump were respected during the idle time. The validation of the duty cycle and power consumption of the chiller was reported both for the machine warm-up phase (the spindle is activated to reach a steady-state thermal condition, fig. 5b) and idle state (fig. 5c).

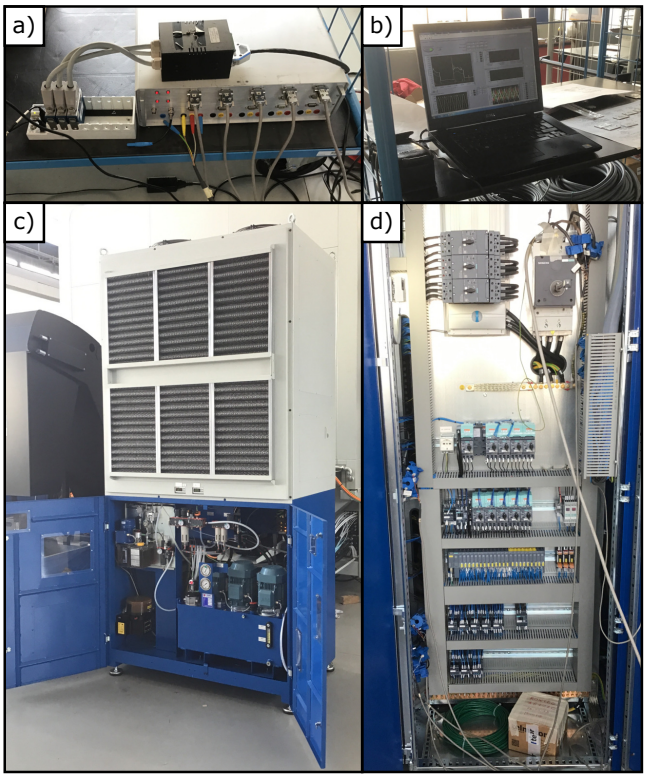

Figure 4. The entire experimental setup: a) DAQ system and power meter; b) LabView® acquisition software; c) Hydraulic unit; d) electrical cabinet and LEM installation

3 Methods

3.1 Synthetic data generation

In the machine tools scenario, collecting fault data could be a difficult task, perhaps infeasible. A digital twin of the system was used to recreate all possible combinations of fault states (fig. 6A) for the components under analysis while operating under different working regimes (fig. 6B), following scientific literature[53–58] and analogously to what Helwig *et al.* did experimentally[11,12,51]. Indeed, in industrial scenarios, machine tools present high flexibility in working conditions. Hydraulic unit working cycles depend on various parameters such as the occurrence of tool changes, the duration of the machining operations and the loading condition (i.e. the heat transferred to the oil from the machine head/spindle during the operation). It is assumed that a single working cycle for PHM could be acceptable when the machine is dedicated to a single task (e.g. in mass-production industries), while this is not the case for most manufacturing companies. Different working regimes can cause dramatic changes in sensor outputs and, as a consequence, in the classification accuracy[11].

Then, as a novelty with respect to typical literature approaches, two kinds of working cycles were simulated to test the robustness of the proposed solution: stationary and non-stationary ones, which represented a machine conceived

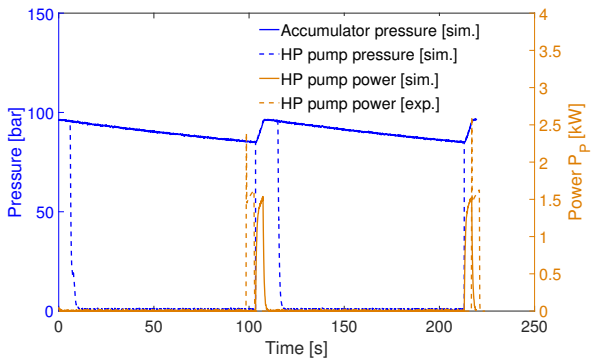

(a) Acquisitions from HP pump of the unit during a healthy behaviour

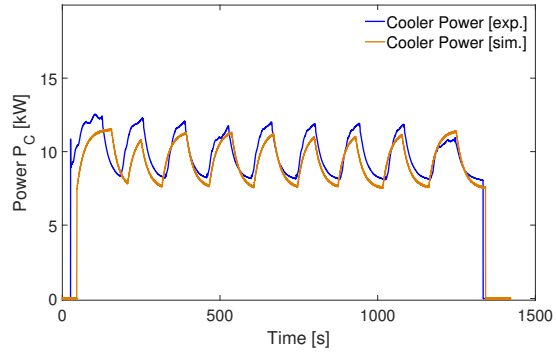

(b) Acquisitions from chiller healthy behaviour in warm-up

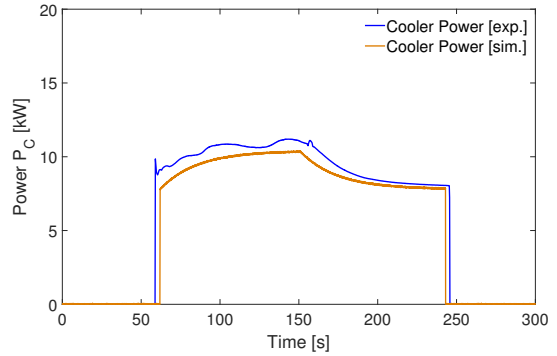

(c) Acquisitions from chiller healthy behaviour in idle state

Figure 5. Comparison between experimental and simulated power

for a specific and a more flexible task, respectively (fig. 6B). Non-stationary cycles were created by mixing stationary cycles in fixed proportions, representing more realistic scenarios for a machine tool. Two stationary (SC1 and SC2) and two non-stationary working cycles (NSC1 and NSC2) were simulated:

- SC1 was composed of 300 seconds of machining (tool clamped) and 15 seconds for tool change (tool released), fig. 7a. The loading condition was represented by the average heat flow of 5kW removed from the head/spindle. This cycle comprised stationary subsequent phases of machining and tool changes;
- SC2 was composed of 150 second and 10 second phases respectively (figure 7b). The average heat flow absorbed by the oil was 3kW.
- NSC1 was composed of 70 percent of SC1 and 30 percent of SC2.
- NSC2 was composed of 30 percent and 70 percent respectively.

Figure 7c represented a qualitative structure of non-stationary cycles. Two datasets were created, one including SC1 and SC2, the other including NSC1 and NSC2. The output of the digital twin consisted of 41 physical quantities, theoretically measurable through sensors to be mounted on the machine. A total of 108 simulations for each dataset were generated combining all the HI listed in table 1. Indeed, the datasets covered all the possible scenarios: all components at full health, single faults and multiple occurring faults.

3.2 Feature extraction

Three global features (from the whole cycle) were extracted for each signal: mean, Skewness and Kurtosis coefficients (fig. 6C). Global features provide a significant reduction of the dimensionality, but in some applications, they are not enough to obtain good results and local ones (from parts of the cycle) should be introduced. The features were then normalised to have null mean and unitary standard deviation[18]. For each fault combination, 20 repetitions were obtained adding random Gaussian noise proportional to signals' RMS. Resulting datasets consisted of 2160 rows and 123 columns (fig. 6D).

3.3 Feature selection/Machine sensorisation

An innovative aspect presented in this paper regards the use of feature selection to obtain useful tips for machine sensorisation. Although applying dimensionality reduction techniques such as Principal Component Analysis or LDA leads to a smaller space to work on, the entire set of features is used and no sensor selection can be done. The proposed feature selection strategy was divided into two steps (fig. 6E). The first was dedicated to sensor selection. The score of each feature with respect to the components was computed separately through the One-Way-ANOVA F-statistic[59]:

$$F_k = \frac{\sum_{j=1}^{r} n_j(\overline{x}_{j,k} - \overline{x}_k)^2/(r-1)}{\sum_{j=1}^{r}\sum_{i=1}^{n_j}(x_{ij,k} - \overline{x}_{j,k})^2/(N-r)} \qquad (19)$$

where r is the number of HI of a component; n_j is the number of samples in the $j-th$ group; $\overline{x}_{j,k}$ is the sample mean of the $k-th$ feature of the $j-th$ group; $\overline{x}_k$ is the mean of the $k-th$ feature; $x_{ij,k}$ is the value of the $k-th$

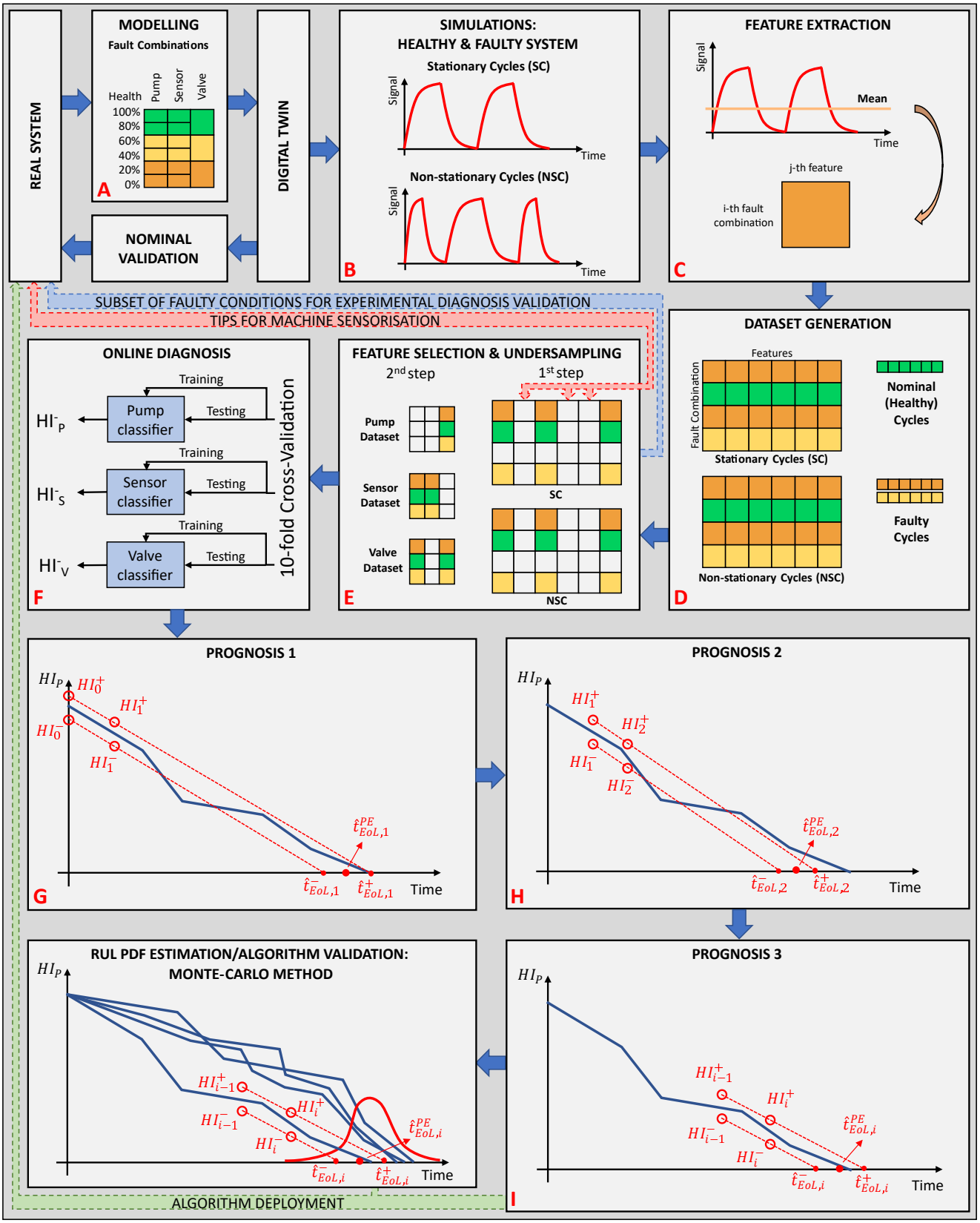

Figure 6. Framework of the whole approach

feature in the $i-th$ repetition of the $j-th$ group; N is the total number of rows of the dataset (fig. 8).

At the same time, the correlation matrix between features was computed, using Pearson's correlation coefficient:

$$\rho_{k,m} = \frac{\mathrm{Cov}(F_k, F_m)}{\sigma_{F_k} \cdot \sigma_{F_m}} \tag{20}$$

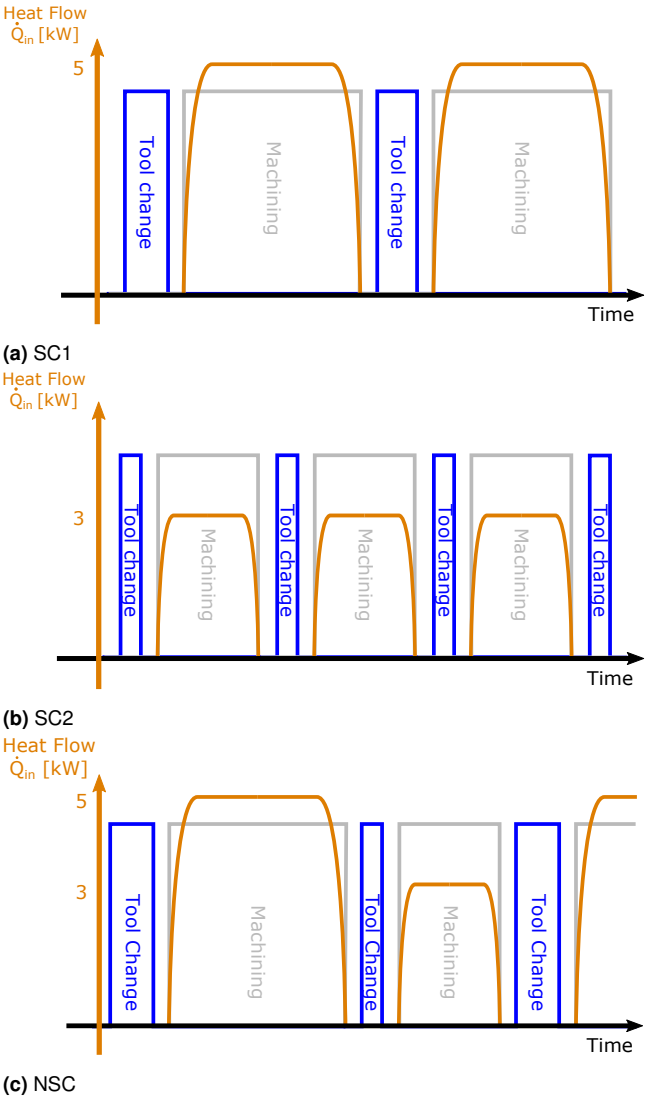

Figure 7. Qualitative structure of the simulated working cycles in terms of machining duty cycle, tool change and heat flow $\dot{Q}_{in}$

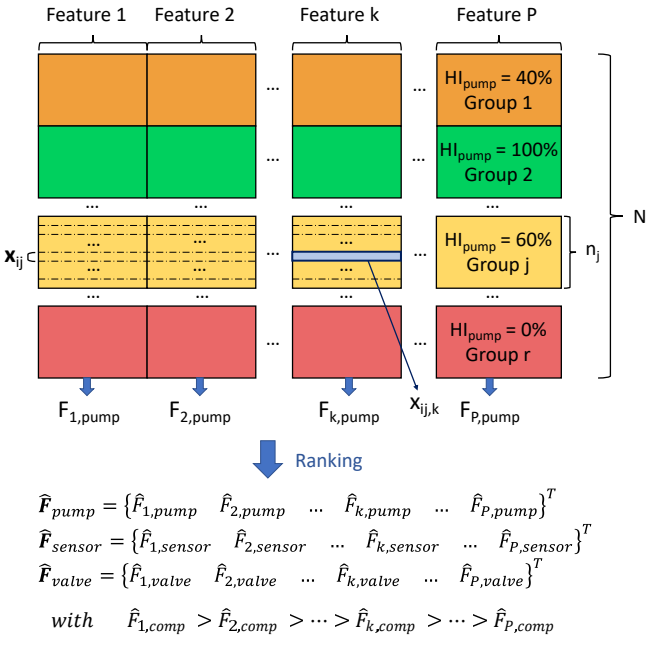

Figure 8. Graphical representation of ANOVA dataset subdivision and scoring

where $\rho_{k,m}$ is the correlation coefficient between the features $k-th$ and $m-th$ one; Cov is the sample covariance between features F_k and F_m; σ_{F_k} and σ_{F_m} are the sample standard deviations of features F_k and F_m. Starting from the feature with the highest score, up to ten features for each component were selected if each correlation with respect to those already selected was below a threshold of 0.4*. A final features pool was created by concatenating selected features for each component and excluding duplicates.

The second step consisted of reiterating the computation of the ANOVA scores only on the new features pool and selecting the best features for each component. The novelty of this approach was not only the use of non-correlated features but also the selection of which feature, and consequently which sensor, provided the most valuable information. This step could have consequences on the design of the machine sensorisation. By identifying the best features for the diagnosis purpose, only useful sensors were traced back: seven sensors were used to compute the selected features pool representing 17% of the initial pool. Only the second step of feature selection was needed for the final implementation of the algorithm.

3.4 Undersampling/Design of experiments

The undersampling technique was applied to reduce the number of experiments for a future validation of the model under faulty conditions. Experimental campaigns can be time-consuming and expensive (e.g. Helwig *et al.* conducted a total of 2,205 tests on a test bench[11]). With regard to the objective of creating an experimental campaign based on the real system, selecting which scenarios to experiment first was needed.

Undersampling, typically applied to imbalanced datasets[62], was extended to identify the most valuable fault combinations for the classification purpose and consequently for the future experimentation on the real machine (fig. 6E). This technique could be applied since a classification model was developed for each component. The dataset was reduced three times (one for each component) and all the shared combinations were stored. In case a particular label is missing after this process, a fault-combination must be reintroduced manually to preserve all the classes of each component. Based on the nearest neighbours rule, *NearMiss*[62], the used undersampling technique selected a

*There is not an absolute value for correlation cut-off. However, in the work proposed by Vatcheva *et al.*, the authors indicated that usually correlation cut-offs for regression can range from 0.5 - 0.8[60]. Here, the idea is to be more conservative, being in a classification scenario. Furthermore, the aim is to also reduce the number of features as much as possible.

Table 2. Time required by different algorithms to perform a 10-fold cross-validation, training and testing of a single sample for each component analysed. The algorithms' complexity is also reported following computational performance metrics[61]: p, number of features; r, number of classes; t, number of trees; N, number of samples; e, number of training epochs; i, j, k, l, number of neurons in each layer.

LDA	10F-CV [s]	Training [s]	Testing [s]	Complexity
Pump	0.190	0.015	<0.001	$\mathcal{O}(rp)$
Sensor	0.189	0.022	<0.001	
Valve	0.160	0.015	<0.001	
RFC	10F-CV [s]	Training [s]	Testing [s]	Complexity
Pump	9.935	0.300	<0.001	$\mathcal{O}(N^2pt)$
Sensor	6.559	0.416	<0.001	
Valve	4.710	0.263	<0.001	
ADB	10F-CV [s]	Training [s]	Testing [s]	Complexity
Pump	8.972	0.579	<0.001	$\mathcal{O}(pNt)$
Sensor	178.669	17.289	0.005	
Valve	362.898	33.593	0.009	
CNN	10F-CV [s]	Training [s]	Testing [s]	Complexity
Pump	68.730	0.858	<0.001	$\mathcal{O}(eN(ij+jk+kl))$
Sensor	97.438	0.900	<0.001	
Valve	125.235	1.094	<0.001	
QDA	10F-CV [s]	Training [s]	Testing [s]	Complexity
Pump	0.213	0.015	<0.001	$\mathcal{O}(p^2r)$
Sensor	0.232	0.015	<0.001	
Valve	0.080	0.010	<0.001	

given number of samples from cluster *A* which were closest to each instance in cluster *B*.

As a result, 41 fault combinations were deleted, representing almost 38% of those that were started with. Undersampling was not needed for the final implementation of the algorithm.

3.5 Diagnostics

In this work, a tailored diagnosis solution was developed for each component fault (figure 6F). In literature, only one algorithm is selected and tuned for all the components under study. Here, a pool of algorithms was selected: LDA, Random Forest Classifier (RFC), Convolutional Neural Network (CNN), Quadratic Discriminant Analysis (QDA) and AdaBoost Classifier (ADB). The application scenario allowed for supervised learning techniques. In fact, the built datasets consisted of features values for known fault combinations (class labels). Two phases were needed: a training procedure, to update classifier parameters on training data, and a testing procedure to evaluate their performances. In order to compare the algorithms and select the most appropriate one for each component, classification accuracy (or classification rate) was introduced due to its easy interpretation. Performances were investigated both on stationary and non-stationary cycles. For the first ones, a 10-fold cross-validation (CV) was selected, according to the literature[20]. The mean of the accuracy was computed for each classification algorithm. For non-stationary cycles, algorithms were trained upon the stationary dataset and tested on the non-stationary one. In this way, the robustness of the solution was validated on unseen and different working regimes. The time required by the algorithms to perform a 10-fold cross-validation, training and testing was reported in table 2, together with their complexity.

The algorithm with the highest final classification rate with respect to a given component was selected as its classifier (in case of a draw, the fastest one was chosen). Diagnosis was then run online at fixed intervals, providing HI as output for the three components.

3.6 Prognostics

The proposed prognosis solution can be applied in case run-to-failures or statistical data are available or not. The two associated procedures and algorithm structures were represented in figure 9.

A novelty of this prognosis approach is that it is based on the output of the diagnosis module, i.e. a set of HI representing the separated health status of the components. Indeed, the approach is able to take into consideration single fault scenarios and multiple occurring faults. By the way,

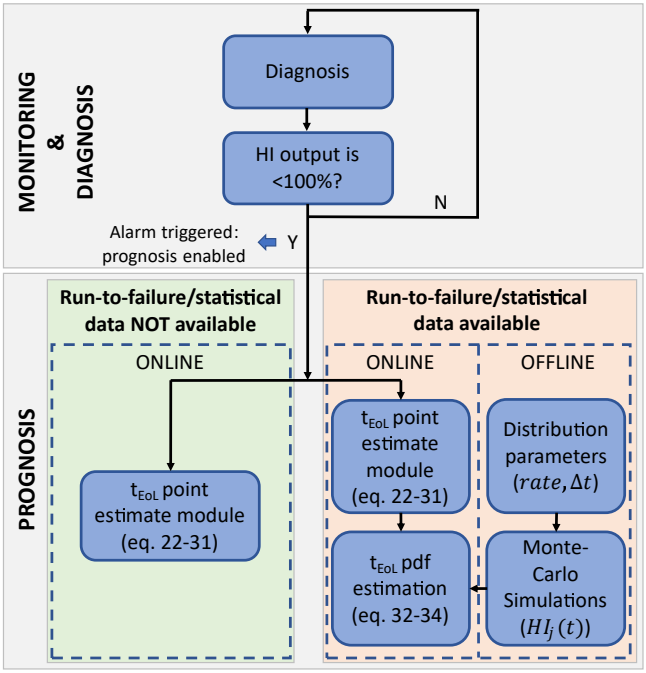

Figure 9. Different strategies for prognosis in the presence, or not, of run-to failure data

it's worth noting that in this way, diagnosis performances have an impact on the prognostics solution. Diagnosis returns, at regular intervals of time Δt_d, a discrete estimate HI^- of the real HI degradation pattern (i.e. ideally the nearest severity used for diagnosis training, figure 10a in red). Discretisation depends on how many fault states the classification algorithms were trained on. The gap between two levels of classified HI is:

$$\delta HI = \frac{100\%}{r-1} \tag{21}$$

where r corresponds to the number of fault states considered. For instance, for the pump leakage, the HI can be classified to be only 0%, 20%, 40%, 60%, 80% or 100% ($\delta HI = 20\%$ and $r = 6$). A prognosis module is generated for each component and acts independently of the others. Furthermore, the prognosis is triggered when the HI goes below 100% (fig. 9). For the sake of clarity, just one model is considered and explained.

3.6.1 End of Life (EoL) time point estimate The procedure in the left branch of fig. 9 could be completely liberated from experimental tests and gives a point estimate of the RUL of a component.

At the end of the degradation process, a monotonic decreasing stair-like HI history is constructed ranging from 100% to 0%. When a new value of the HI is available, it is compared to the previous one. A set of three variables t_i, $HI^-(t_i)$ and $HI^+(t_i)$ (eq. 24) was stored whenever:

$$HI^-(t_i) < HI^-(t_i - \Delta t_d) \tag{22}$$

and holds:

$$t_i = k_i \Delta t_d \tag{23}$$

$$HI^+(t_i) = HI^-(t_i) + \delta HI \tag{24}$$

with $i = 0, \ldots, r-1$ (fig 10a). At the end of the component life, a set of r instants and r pairs of HI were collected (starting from the instant $t_0 = 0$, $HI_0^- = 100\%$ and $HI_0^+ = 100\% + \delta HI$).

Except for the starting time instant t_0, at any t_i, an updated estimation of the EoL time is performed as follows (fig. 6G-H-I):

1. Compute the line between the last two HI^+ and HI^- as a function of time t:

$$HI^-(t) = \frac{HI^-(t_i) - HI^-(t_{i-1})}{t_i - t_{i-1}}(t - t_i) + HI^-(t_i) \tag{25}$$

$$HI^+(t) = \frac{HI^+(t_i) - HI^+(t_{i-1})}{t_i - t_{i-1}}(t - t_i) + HI^+(t_i) \tag{26}$$

   with $i = 1, \ldots, r-1$.
2. Compute the EoL estimates imposing:

$$HI^-(\hat{t}^-_{EoL,i}) = 0 \tag{27}$$

$$HI^+(\hat{t}^+_{EoL,i}) = 0 \tag{28}$$

   from which:

$$\hat{t}^-_{EoL,i} = t_i - HI^-(t_i)\frac{t_i - t_{i-1}}{HI^-(t_i) - HI^-(t_{i-1})} \tag{29}$$

$$\hat{t}^+_{EoL,i} = t_i - HI^+(t_i)\frac{t_i - t_{i-1}}{HI^+(t_i) - HI^+(t_{i-1})} \tag{30}$$

   with $i = 1, \ldots, r-1$.
3. Compute the unbiased $i-th$ point estimate for the EoL time:

$$\hat{t}^{PE}_{EoL,i} = \frac{\hat{t}^-_{EoL,i} + \hat{t}^+_{EoL,i}}{2} \tag{31}$$

   with $i = 1, \ldots, r-1$.

The last step is necessary since $\hat{t}^-_{EoL,i}$ tends to underestimate the real EoL time, while $\hat{t}^+_{EoL,i}$ tends to overestimate it.

3.6.2 Monte Carlo RUL pdf estimation If run-to-failure tests or statistical data were available, a statistical method for RUL pdf estimation is obtained through the Monte Carlo approach in the right branch of fig. 9. This method is based on the definition of a monotonic decreasing piecewise

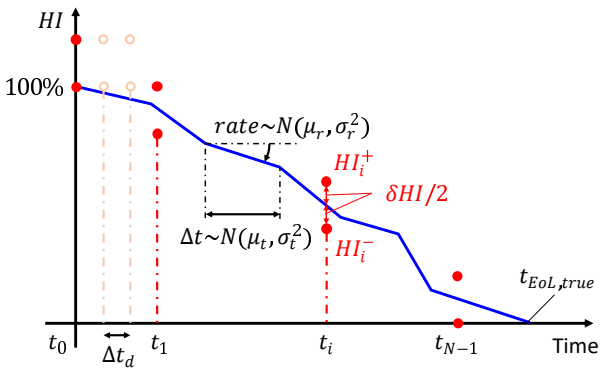

(a) The actual value of HI is represented by the solid line. Dots represent the HI_i at the time instant t_i. Parameters Δt and *rate* sampled from their distributions in any Monte Carlo simulation are shown

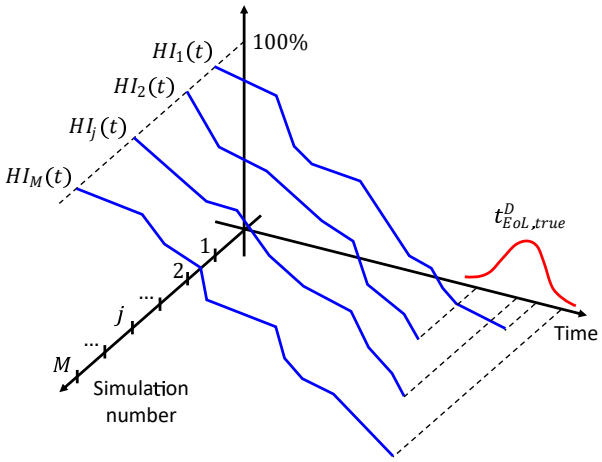

(b) Monte Carlo simulations of M $HI(t)$

Figure 10. Monte Carlo graphical representation

function which represents the "real" degradation trend of the HI of a component fault. This is true when a linear degradation pattern with different working loads is operated on the machine. The Monte Carlo approach was designed to extract a set of M completely new degradation patterns (Monte Carlo simulations) $HI_j(t)$ with $j = 1, 2, ..., M$ (see figure 10b). The variability was introduced by sampling the degradation *rate* of each single piece of the function from a Gaussian distribution and sampling the duration of each single piece Δt from another Gaussian distribution (see figure 10a). Applying equations 22-31 to all the M Monte Carlo samples, it was possible to extract the distribution relative to the $i-th$ EoL point estimate as the collection of the $\hat{t}^{PE}_{EoL,i,j}$. It was also possible to define all the last time instants of the real patterns $HI_j(t)$:

$$t_{EoL,true,j} \Rightarrow HI_j(t = t_{EoL,true,j}) = 0 \qquad (32)$$

with $j = 1, 2, ..., M$ and their collection $t^D_{EoL,true}$. The prediction error is defined as:

$$e_{i,j} = \frac{\hat{t}^{PE}_{EoL,i,j} - t_{EoL,true,j}}{\hat{t}^{PE}_{EoL,i,j}} \qquad (33)$$

while the error distribution associated with the $i-th$ estimate e^D_i is the collection of the $e_{i,j}$ with $j = 1, 2, \ldots, M$. t_{EoL} pdf can instead be computed as:

$$\hat{t}^D_{EoL,i} = \hat{t}^{PE}_{EoL,i}(1 - e^D_i) \qquad (34)$$

The described Monte Carlo approach (up to eq. 33) was used to test the performances of the point estimate module, either in terms of estimation error mean or variance. Here, distributions shown in figure 10a were hypothesised.

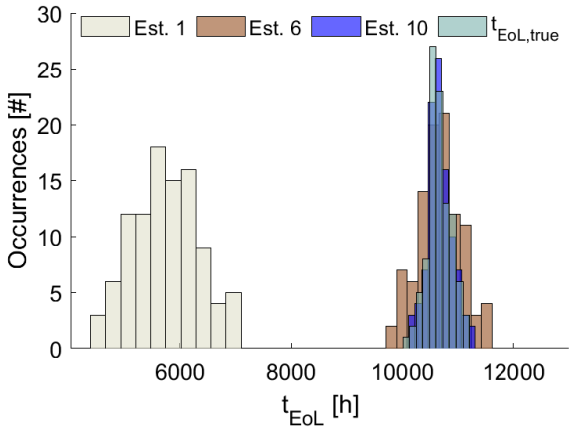

Figure 11. Estimates distribution of t_{EoL} evolution with respect to the estimate number. Note that the estimates are ten but just three are shown in order not to make graphical confusion due to superimposition. Also, the distribution of the real EoL time of Monte Carlo samples is shown

4 Results

4.1 Diagnosis

Diagnosis results for all types of working cycle were shown in table 3. The column labels are explained in the following:

- SC12: classification rates for each component based on 10-fold CV for stationary working cycles 1 and 2;
- NSC1 and NSC2: classification rates for non-stationary working cycles with training done using stationary working cycles 1 and 2;
- suffix FS indicates that the classification rates were obtained with the application of the feature selection.

4.2 Prognosis

In order to evaluate the performances of the algorithm, a Monte Carlo based analysis was carried out. In figure 11,

Table 3. Classification rates of the five best algorithms.

LDA	SC12	NSC1	NSC2	SC12 FS	NSC1 FS	NSC2 FS
Pump	100.00%	99.79%	99.42%	100.00%	100.00%	99.98%
Sensor	64.14%	78.03%	76.23%	65.79%	75.21%	77.50%
Valve	72.18%	76.85%	69.91%	72.31%	79.00%	75.97%
RFC	SC12	NSC1	NSC2	SC12 FS	NSC1 FS	NSC2 FS
Pump	95.88%	97.62%	96.50%	100.00%	100.00%	100.00%
Sensor	79.10%	56.85%	56.60%	79.10%	56.85%	56.60%
Valve	88.10%	67.94%	60.74%	88.10%	67.94%	60.74%
ADB	SC12	NSC1	NSC2	SC12 FS	NSC1 FS	NSC2 FS
Pump	100.00%	99.91%	99.79%	100.00%	100.00%	100.00%
Sensor	69.84%	70.84%	79.84%	71.32%	74.28%	76.62%
Valve	73.73%	77.34%	74.05%	73.73%	77.34%	74.05%
CNN	SC12	NSC1	NSC2	SC12 FS	NSC1 FS	NSC2 FS
Pump	99.49%	100.00%	99.76%	99.98%	100.00%	99.97%
Sensor	81.23%	79.67%	85.16%	79.75%	90.94%	82.61%
Valve	76.62%	77.61%	77.82%	74.93%	81.62%	81.57%
QDA	SC12	NSC1	NSC2	SC12 FS	NSC1 FS	NSC2 FS
Pump	96.76%	99.86%	99.00%	100.00%	100.00%	100.00%
Sensor	63.70%	49.75%	54.98%	70.12%	66.18%	73.87%
Valve	71.13%	81.27%	75.51%	71.41%	79.00%	76.41%

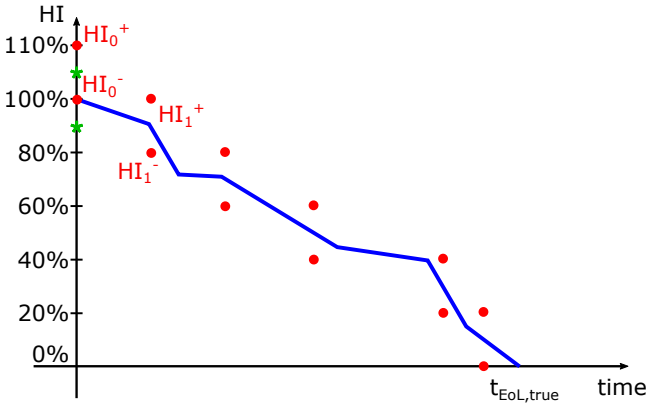

Figure 12. The underestimation problem of the first estimate is due to the different selection criteria of the HI_0^+ and HI_0^-. The corrected HI are shown by asterisks

the evolution of the EoL time distributions with respect to the estimation number were shown. Parameters of the distributions shown in figure 10a were hypothesised. As expected, as long as the time of the estimate is approaching the real End-of-Life time of the component, the distributions of the estimated EoL time are getting better, both in terms of expected value and variance. It is worth noting that the first estimate is underestimating the real EoL time. This is due to the fact that, at time instant $t_0 = 0$, the algorithm is considering $HI_0^- = 100\%$ and $HI_0^+ = 100\% + \delta HI$. This leads to an overestimation of the real $HI(t)$ pattern (fig. 12). At $t_0 = 0$, HI^- is coincident with the real pattern, while in other t_i, the real pattern is exactly the mean value of HI_i^- and HI_i^+. This operation is lifting up the first point of the pair over which the linear interpolation is computed at t_1. The overestimated pair of HI then leads to an excessively negative predicted rate of degradation which turns into an underestimation of the RUL. This issue can be easily addressed by adding a correction term in HI_0^- and HI_0^+:

$$HI_0^- = 100\% - \frac{\delta HI}{2} \tag{35}$$

$$HI_0^+ = 100\% + \frac{\delta HI}{2} \tag{36}$$

By adopting this correction, the lift effect due to the first HI, overestimation could be softened. However, the prognostic solution was, estimate by estimate, converging on the true EoL time. Such a phenomenon was also evident in the distribution of the prediction errors. In figure 13, the bias of the first estimate is evident, while the progression of the estimate is reducing the errors. The error mean and the 95% interval of error trends during the life of the component were plotted and showed the tendency to become null and decrease respectively over the time. Furthermore, the behaviour of the algorithm with respect to the different number of levels adopted in the classification procedure was analysed. In this case, 7, 9, 10, 11 and 13 levels of classifiers were tested.

In figure 13, an insignificant difference between the different classifiers is shown: the classifier with the lowest number of fault states shows slightly smaller error intervals, but at the same time, the last estimate is much earlier during

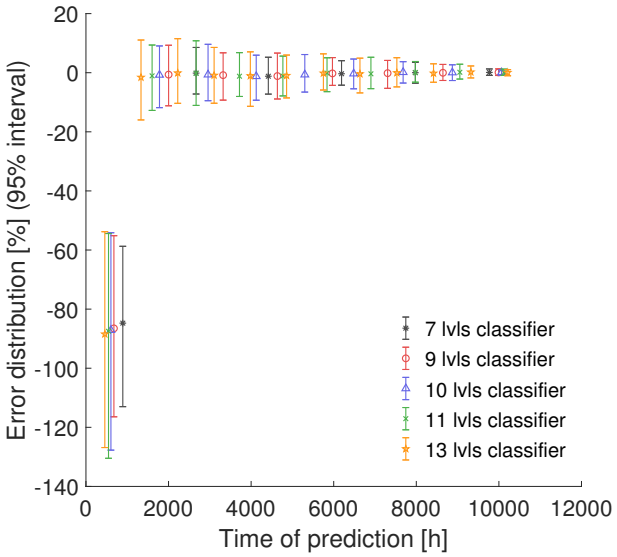

Figure 13. 95% error intervals for different classifiers during a component's life. Five different classifiers are tested with 7, 9, 10, 11, 13 fault states

the life of the component. In this way, the last estimate of the classifiers with a higher number of fault states are further towards the component EoL allowing a narrower error interval (note that the first estimate is performed earlier but with a bigger error interval). On the other hand, classifiers with a higher number of fault states, require a higher number of tests for training and tend to be more critical in the diagnosis phase. Analysis of performances of the algorithm with respect to other distributions is out of the scope of this paper and will be a matter for future work by the authors.

5 Conclusions

In this paper, a PHM solution for a machine tool hydraulic unit was presented. Despite the hydraulic unit being one of the most critical part of machine tools [1,3,36], scientific literature was still lacking in this research field. The unavailability of a large amount of faulty data in the life of a machine tool brought about the decision to implement a digital twin of the hydraulic unit. The model was used to generate simulations of the healthy and faulty machine during multiple working cycles:

- such a solution was demonstrated to be efficient in addressing the working regime variability, i.e. the main limitation for the applicability of prognosis approaches in industry;
- the use of a digital twin allowed the support of the sensorisation and the design of experiments for a future validation of the model under fault conditions;
- a tailored multi-classifier solution was developed for any component, whereas typical literature solutions are based on a single classifier approach. QDA performed an excellent pump fault diagnosis, while CNN was the best classifier for sensor and valve faults.
- the proposed prognosis solution took into account the interaction between different faults, exploiting diagnosis outputs trained on all the fault combinations.
- the developed algorithm was able to estimate the RUL probability density function through a Monte Carlo approach.

Proposals for future works include the deployment of the algorithm on a test rig of the system, experimental validation of the digital twin in the presence of faults based on feature selection and undersampling support, and robustness tests on new and unseen working cycles.

Acknowledgements

The authors would like to thank MANDELLI SISTEMI S.P.A. for their contribution to the project.

Declaration of conflicting interests

The authors declare that they have no known competing financial interests or personal relationships that could have appeared to influence the work reported in this paper.

Funding

The project was funded by the Ministero dello Sviluppo Economico (MISE) - Industria Sostenibile FRI–DM 24/07/2015– (Project ref. 55 - B38I17000590008).

Supplemental material

Not applicable.

ORCID iDs

Luca Bernini: 0000-0002-7064-7518
David Waltz: 0000-0001-9534-9077
Paolo Albertelli: 0000-0001-5098-0420
Michele Monno: 0000-0002-1957-3613

References

1. Chen F, Chen X, Xie Q et al. Reliability Analysis of Numerical Control Lathe Based On The Field Data. In *Proceedings of the 2015 6th International Conference on Manufacturing Science and Engineering*. Atlantis Press, pp. 1018–1024. DOI:10.2991/icmse-15.2015.185. URL https://doi.org/10.2991/icmse-15.2015.185.

2. Ferreiro S, Konde E, Fernández S et al. INDUSTRY 4.0: Predictive Intelligent Maintenance for Production Equipment. In *European Conference of the Prognostics and Health Management Society*. June 2016, pp. 1–8.
3. Patil RB and Kothavale BS. Failure Modes and Effects Analysis (FMEA) of Computerized Numerical Control (CNC) Turning Center. *International Review of Mechanical Engineering (IREME)* 2018; 12(1): 78–87. DOI:10.15866/ireme.v12i1.14156. URL https://doi.org/10.15866/ireme.v12i1.14156.
4. Jardine AK, Lin D and Banjevic D. A review on machinery diagnostics and prognostics implementing condition-based maintenance. *Mechanical Systems and Signal Processing* 2006; 20(7): 1483–1510. DOI:10.1016/j.ymssp.2005.09.012. URL https://doi.org/10.1016/j.ymssp.2005.09.012.
5. ISO Central Secretary. Condition monitoring and diagnostics of machines - Data interpretation and diagnostics techniques - Part 1: General guidelines. Standard ISO 13379-1:2012. International Organization for Standardization, Geneva, CH 2012; .
6. ISO Central Secretary. Condition monitoring and diagnostics of machines - Data interpretation and diagnostics techniques - Part 2: Data-driven applications. Standard ISO 13379-2:2015. International Organization for Standardization, Geneva, CH 2015; .
7. ISO Central Secretary. Condition Monitoring and Diagnostics of Machines - Prognostics - Part 1: General Guidelines. Standard ISO 13381-1:2015. International Organization for Standardization, Geneva, CH 2015; .
8. ISO Central Secretary. Condition monitoring and diagnostics of machines - General guidelines. Standard ISO 17359:2018. International Organization for Standardization, Geneva, CH 2018; .
9. ISO Central Secretary. Quality management systems - Requirements. Standard ISO 9001:2015. International Organization for Standardization, Geneva, CH 2015; .
10. Baur M, Albertelli P and Monno M. A review of prognostics and health management of machine tools. *The International Journal of Advanced Manufacturing Technology* 2020; 107(5): 2843–2863. DOI:10.1007/s00170-020-05202-3. URL https://doi.org/10.1007/s00170-020-05202-3.
11. Helwig N, Pignanelli E and Schütze A. Condition monitoring of a complex hydraulic system using multivariate statistics. In *2015 IEEE International Instrumentation and Measurement Technology Conference (I2MTC) Proceedings*. pp. 210–215. DOI:10.1109/I2MTC.2015.7151267. URL https://doi.org/10.1109/I2MTC.2015.7151267.
12. Helwig N, Klein S and Schütze A. Identification and Quantification of Hydraulic System Faults Based on Multivariate Statistics Using Spectral Vibration Features. *Procedia Engineering* 2015; 120: 1225–1228. DOI:10.1016/j.proeng.2015.08.835. URL https://doi.org/10.1016/j.proeng.2015.08.835.
13. Gilioli A, Sbarufatti C, Manes A et al. Compression after impact test (CAI) on NOMEX™ honeycomb sandwich panels with thin aluminum skins. *Composites Part B: Engineering* 2014; 67: 313–325. DOI:10.1016/j.compositesb.2014.07.015. URL https://doi.org/10.1016/j.compositesb.2014.07.015.
14. Montgomery DC. *Introduction to Statistical Quality Control*. Sixth ed. John Wiley & Sons, Inc., 2008. ISBN 978-0-470-16992-6.
15. Liu J, Djurdjanovic D, Marko K et al. Growing Structure Multiple Model Systems for Anomaly Detection and Fault Diagnosis. *Journal of Dynamic Systems, Measurement, and Control* 2009; 131(5). DOI:10.1115/1.3155004. URL https://doi.org/10.1115/1.3155004.
16. Colosimo B, Moroni G and Grasso M. Real-time tool condition monitoring in milling by means of control charts for auto-correlated data. *Journal of Machine Engineering* 2010; 10: 5–17.
17. Khorsheed RM and Beyca OF. An integrated machine learning: Utility theory framework for real-time predictive maintenance in pumping systems. *Proceedings of the Institution of Mechanical Engineers, Part B: Journal of Engineering Manufacture* 2021; 235(5): 887–901. DOI:10.1177/0954405420970517. URL https://doi.org/10.1177/0954405420970517.
18. Soylemezoglu A, Jagannathan S and Saygin C. Mahalanobis-Taguchi System as a Multi-Sensor Based Decision Making Prognostics Tool for Centrifugal Pump Failures. *IEEE Transactions on Reliability* 2011; 60(4): 864–878. DOI:10.1109/TR.2011.2170255. URL https://doi.org/10.1109/TR.2011.2170255.
19. Razavi B and De Silva CW. Condition Monitoring in a Hydraulic System of an Industrial Machine Using Unscented Kalman Filter. *International Journal of Information Acquisition* 2010; 07(03): 177–192. DOI:10.1142/S0219878910002191. URL https://doi.org/10.1142/S0219878910002191.
20. Hastie T, Tibshirani R and Friedman J. *The Elements of Statistical Learning: Data Mining, Inference, and Prediction*. Second ed. New York: Springer, 2009. ISBN 978-0-387-84857-0. DOI:10.1007/978-0-387-84858-7. URL https://doi.org/10.1007/978-0-387-84858-7.

21. Zuo GL, Lai SD and Cheng Y. Study on the Fault Diagnosis of Gear Pump Based on PNN Neural Network. *Advanced Materials Research* 2014; 1044: 873–876. DOI: 10.4028/www.scientific.net/AMR.1044-1045.873. URL https://doi.org/10.4028/www.scientific.net/AMR.1044-1045.873.
22. Venkatesan R and Er MJ. A novel progressive learning technique for multi-class classification. *Neurocomputing* 2016; 207: 310–321. DOI:10.1016/j.neucom.2016.05.006. URL https://doi.org/10.1016/j.neucom.2016.05.006.
23. Peng Y, Dong M and Zuo MJ. Current status of machine prognostics in condition-based maintenance: a review. *The International Journal of Advanced Manufacturing Technology* 2010; 50(1): 297–313. DOI:10.1007/s00170-009-2482-0. URL https://doi.org/10.1007/s00170-009-2482-0.
24. Cheng Q, Qi B, Liu Z et al. Positioning accuracy degradation and lifetime prediction of the ball screw considering time-varying working conditions and feed modes. *Proceedings of the Institution of Mechanical Engineers, Part B: Journal of Engineering Manufacture* 2021; 235(6-7): 943–957. DOI: 10.1177/0954405420971089. URL https://doi.org/10.1177/0954405420971089.
25. Zhao P, Cheng K, Jiang B et al. Development of the innovative differential tool wear modeling for high-feed milling and its experimental verification. *Proceedings of the Institution of Mechanical Engineers, Part B: Journal of Engineering Manufacture* 2021; 235(1-2): 85–97. DOI:10.1177/0954405420949226. URL https://doi.org/10.1177/0954405420949226.
26. Sagar CK, Priyadarshini A, Gupta AK et al. Experimental investigation of tool wear characteristics and analytical prediction of tool life using a modified tool wear rate model while machining 90 tungsten heavy alloys. *Proceedings of the Institution of Mechanical Engineers, Part B: Journal of Engineering Manufacture* 2021; 235(1-2): 242–254. DOI: 10.1177/0954405420933113. URL https://doi.org/10.1177/0954405420933113.
27. Gomes JPP, Leão BP, Vianna WO et al. Failure prognostics of a hydraulic pump using Kalman Filter. *Proceedings of the Annual Conference of the Prognostics and Health Management Society 2012* 2012; 4(1): 464–468.
28. Gomes JP, Rodrigues LR, Leão BP et al. Using Degradation Messages to Predict Hydraulic System Failures in a Commercial Aircraft. *IEEE Transactions on Automation Science and Engineering* 2018; 15(1): 214–224. DOI:10.1109/TASE.2016.2601261. URL https://doi.org/10.1109/TASE.2016.2601261.
29. Wang D and Tse PW. Prognostics of slurry pumps based on a moving-average wear degradation index and a general sequential Monte Carlo method. *Mechanical Systems and Signal Processing* 2015; 56-57: 213–229. DOI:10.1016/j.ymssp.2014.10.010. URL https://doi.org/10.1016/j.ymssp.2014.10.010.
30. Liao L, Wang H and Lee J. Bearing Health Assessment and Fault Diagnosis Using the Method of Self-Organizing Map. In *2007 61st Meeting of the Society for Machinery Failure Prevention Technology*.
31. de Oliveira Bizarria C and Yoneyama T. Prognostics and Health Monitoring for an electro-hydraulic flight control actuator. In *2009 IEEE Aerospace conference*. IEEE, pp. 1–9. DOI:10.1109/AERO.2009.4839658. URL https://doi.org/10.1109/AERO.2009.4839658.
32. Cholette ME, Liu J, Djurdjanovic D et al. Monitoring of complex systems of interacting dynamic systems. *Applied Intelligence* 2012; 37(1): 60–79. DOI:10.1007/s10489-011-0313-0. URL https://doi.org/10.1007/s10489-011-0313-0.
33. Timusk M, Lipsett M and Mechefske CK. Fault detection using transient machine signals. *Mechanical Systems and Signal Processing* 2008; 22(7): 1724–1749. DOI:10.1016/j.ymssp.2008.01.013. URL https://doi.org/10.1016/j.ymssp.2008.01.013.
34. Hu J and Tse PW. A Relevance Vector Machine-Based Approach with Application to Oil Sand Pump Prognostics. *Sensors* 2013; 13(9): 12663–12686. DOI:10.3390/s130912663. URL https://doi.org/10.3390/s130912663.
35. Sbarufatti C, Corbetta M, Giglio M et al. Adaptive prognosis of lithium-ion batteries based on the combination of particle filters and radial basis function neural networks. *Journal of Power Sources* 2017; 344: 128–140. DOI:10.1016/j.jpowsour.2017.01.105. URL https://doi.org/10.1016/j.jpowsour.2017.01.105.
36. Yang Zj, Chen Ch, Chen F et al. Reliability analysis of machining center based on the field data. *Eksploatacja i Niezawodnosc* 2013; 15(2): 147–155.
37. Gittler T, Gontarz A, Weiss L et al. A fundamental approach for data acquisition on machine tools as enabler for analytical Industrie 4.0 applications. *Procedia CIRP* 2019; 79: 586–591. DOI:10.1016/j.procir.2019.02.088. URL https://doi.org/10.1016/j.procir.2019.02.088.
38. Gittler T, Stoop F, Kryscio D et al. Condition monitoring system for machine tool auxiliaries. *Procedia CIRP* 2020; 88: 358–363. DOI:10.1016/j.procir.2020.05.062. URL https://doi.org/10.1016/j.procir.2020.05.062.

39. Nouri M, Fussell BK, Ziniti BL et al. Real-time tool wear monitoring in milling using a cutting condition independent method. *International Journal of Machine Tools and Manufacture* 2015; 89: 1–13. DOI:10.1016/j.ijmachtools.2014.10.011. URL https://doi.org/10.1016/j.ijmachtools.2014.10.011.
40. Cheng M, Jiao L, Shi X et al. An intelligent prediction model of the tool wear based on machine learning in turning high strength steel. *Proceedings of the Institution of Mechanical Engineers, Part B: Journal of Engineering Manufacture* 2020; 234(13): 1580–1597. DOI:10.1177/0954405420935787. URL https://doi.org/10.1177/0954405420935787.
41. McLeay T, Turner MS and Worden K. A novel approach to machining process fault detection using unsupervised learning. *Proceedings of the Institution of Mechanical Engineers, Part B: Journal of Engineering Manufacture* 2021; 235(10): 1533–1542. DOI:10.1177/0954405420937556. URL https://doi.org/10.1177/0954405420937556.
42. da Silva L, Del Claro V, Andrade C et al. Tool wear monitoring in drilling of high-strength compacted graphite cast irons. *Proceedings of the Institution of Mechanical Engineers, Part B: Journal of Engineering Manufacture* 2021; 235(1-2): 207–218. DOI:10.1177/0954405420937857. URL https://doi.org/10.1177/0954405420937857.
43. Tobon-Mejia DA, Medjaher K and Zerhouni N. CNC machine tool's wear diagnostic and prognostic by using dynamic Bayesian networks. *Mechanical Systems and Signal Processing* 2012; 28: 167–182. DOI:10.1016/j.ymssp.2011.10.018. URL https://doi.org/10.1016/j.ymssp.2011.10.018.
44. Yu J, Liang S, Tang D et al. A weighted hidden Markov model approach for continuous-state tool wear monitoring and tool life prediction. *The International Journal of Advanced Manufacturing Technology* 2017; 91(1): 201–211. DOI:10.1007/s00170-016-9711-0. URL https://doi.org/10.1007/s00170-016-9711-0.
45. Chen X, Song Z, Li H et al. Research on fault early warning and the diagnosis of machine tools based on energy fault tree analysis. *Proceedings of the Institution of Mechanical Engineers, Part B: Journal of Engineering Manufacture* 2019; 233(11): 2147–2159. DOI:10.1177/0954405418816848. URL https://doi.org/10.1177/0954405418816848.
46. Moore J, Stammers J and Dominguez-Caballero J. The application of machine learning to sensor signals for machine tool and process health assessment. *Proceedings of the Institution of Mechanical Engineers, Part B: Journal of Engineering Manufacture* 2021; 235(10): 1543–1557. DOI:10.1177/0954405420960892. URL https://doi.org/10.1177/0954405420960892.
47. Xia Y, Wang W, Song Z et al. Fault diagnosis of flexible production line machining center based on PCA and ABC-LVQ. *Proceedings of the Institution of Mechanical Engineers, Part B: Journal of Engineering Manufacture* 2021; 235(4): 594–604. DOI:10.1177/0954405420970513. URL https://doi.org/10.1177/0954405420970513.
48. Sardana D, Bhatnagar R, Pavel R et al. Data driven predictive analytics for a spindle's health. In *2015 IEEE International Conference on Big Data (Big Data)*. IEEE, pp. 1378–1387. DOI:10.1109/BigData.2015.7363898. URL https://doi.org/10.1109/BigData.2015.7363898.
49. Soylemezoglu A, Jagannathan S and Saygin C. Mahalanobis Taguchi System (MTS) as a Prognostics Tool for Rolling Element Bearing Failures. *Journal of Manufacturing Science and Engineering* 2010; 132(5). DOI:10.1115/1.4002545. URL https://doi.org/10.1115/1.4002545.
50. Jia P, Rong Y and Huang Y. Condition monitoring of the feed drive system of a machine tool based on long-term operational modal analysis. *International Journal of Machine Tools and Manufacture* 2019; 146: 103454. DOI:10.1016/j.ijmachtools.2019.103454. URL https://doi.org/10.1016/j.ijmachtools.2019.103454.
51. Helwig N, Pignanelli E and Schütze A. Detecting and Compensating Sensor Faults in a Hydraulic Condition Monitoring System. In *SENSOR 2015*. pp. 641–646. DOI:10.5162/sensor2015/D8.1. URL https://doi.org/10.5162/sensor2015/D8.1.
52. Rydberg KE. *Hydraulic Servo Systems: Dynamic Properties and Control*. Linköping: Linköping University Electronic Press, 2016. ISBN 9789176856208.
53. Villalobos O, Burvill C and Stecki J. FAULT DIAGNOSIS OF ELECTROHYDRAULIC SYSTEMS. *Proceedings of the JFPS International Symposium on Fluid Power* 2005; 2005(6): 658–663. DOI:10.5739/isfp.2005.658. URL https://doi.org/10.5739/isfp.2005.658.
54. Lamoureux B, Massé JR and Mechbal N. Diagnostics of an aircraft engine pumping unit using a hybrid approach based-on surrogate modeling. In *2013 IEEE Conference on Prognostics and Health Management (PHM)*. pp. 1–8. DOI:10.1109/ICPHM.2013.6621430. URL https://doi.org/10.1109/ICPHM.2013.6621430.
55. Medjaher K and Zerhouni N. Framework for a Hybrid Prognostics. *Chemical Engineering Transactions* 2013; 33: 91–96. DOI:10.3303/CET1333016. URL https://doi.org/10.3303/CET1333016.
56. Sbarufatti C, Manson G and Worden K. A numerically-enhanced machine learning approach to damage diagnosis using a Lamb wave sensing network. *Journal of Sound and Vibration* 2014; 333(19): 4499–4525. DOI:10.1016/j.

jsv.2014.04.059. URL https://doi.org/10.1016/j.jsv.2014.04.059.

57. Leturiondo U, Salgado O, Ciani L et al. Architecture for hybrid modelling and its application to diagnosis and prognosis with missing data. *Measurement* 2017; 108: 152–162. DOI: 10.1016/j.measurement.2017.02.003. URL https://doi.org/10.1016/j.measurement.2017.02.003.
58. Aivaliotis P, Georgoulias K and Chryssolouris G. The use of Digital Twin for predictive maintenance in manufacturing. *International Journal of Computer Integrated Manufacturing* 2019; 32(11): 1067–1080. DOI:10.1080/0951192X.2019.1686173. URL https://doi.org/10.1080/0951192X.2019.1686173.
59. Montgomery DC. *Design and Analysis of Experiments*. Eighth ed. John Wiley & Sons, Inc., 2012. ISBN 9781118214718.
60. Vatcheva KP, Lee M, McCormick JB et al. Multicollinearity in Regression Analyses Conducted in Epidemiologic Studies. *Epidemiology* 2016; 6(2): 227. DOI:10.4172/2161-1165.1000227. URL https://doi.org/10.4172/2161-1165.1000227.
61. Saxena A, Celaya J, Saha B et al. Metrics for Offline Evaluation of Prognostic Performance. *International Journal of Prognostics and Health Management* 2010; 1: 2153–2648. DOI:10.36001/ijphm.2010.v1i1.1336. URL https://doi.org/10.36001/ijphm.2010.v1i1.1336.
62. Beckmann M, Ebecken NFF and Pires de Lima BSL. A KNN Undersampling Approach for Data Balancing. *Journal of Intelligent Learning Systems and Applications* 2015; 07: 104–116. DOI:10.4236/jilsa.2015.74010. URL https://doi.org/10.4236/jilsa.2015.74010.